HAL
open science

Multi-Scale Numerical Analysis of the Effect of Microstructural Features on the Mechanical Behavior of Polycrystalline Ti-6Al-4V Alloy

Fatna Benmessaoud, Vincent Velay, Mohammed Cheikh, Vanessa Vidal, Christine Boher, Farhad Rezai-Aria

To cite this version:

Fatna Benmessaoud, Vincent Velay, Mohammed Cheikh, Vanessa Vidal, Christine Boher, et al.. Multi-Scale Numerical Analysis of the Effect of Microstructural Features on the Mechanical Behavior of Polycrystalline Ti-6Al-4V Alloy. Chemical Engineering Transactions, 2019, 67 (2), pp.227 - 242. 10.24423/EngTrans.1014.20190615 . hal-02201384

HAL Id: hal-02201384

https://imt-mines-albi.hal.science/hal-02201384

Submitted on 31 Jul 2019

HAL is a multi-disciplinary open access archive for the deposit and dissemination of scientific research documents, whether they are published or not. The documents may come from teaching and research institutions in France or abroad, or from public or private research centers.

L'archive ouverte pluridisciplinaire **HAL**, est destinée au dépôt et à la diffusion de documents scientifiques de niveau recherche, publiés ou non, émanant des établissements d'enseignement et de recherche français ou étrangers, des laboratoires publics ou privés.

Distributed under a Creative Commons Attribution - ShareAlike 4.0 International License

Engineering Transactions, **67**(2): 227–242, 2019, doi: 10.24423/EngTrans.1014.20190615
Polish Academy of Sciences • Institute of Fundamental Technological Research (IPPT PAN)
Université de Lorraine • Poznan University of Technology

Multi-Scale Numerical Analysis of the Effect of Microstructural Features on the Mechanical Behavior of Polycrystalline Ti-6Al-4V Alloy

Fatna BENMESSAOUD, Vincent VELAY, Mohammed CHEIKH*
Vanessa VIDAL, Christine BOHER, Farhad RÉZAÏ-ARIA

ICA, Université de Toulouse, CNRS, IMT Mines Albi, INSA, UPS, ISAE-SUPAERO
Compus Jarlard, Albi 81000, France
*Corresponding Author e-mail: mcheikh@univ-tlse2.fr

The present work aims to model the influence of microstructural features of Ti-6Al-4V titanium alloy on its mechanical behavior. A multi-scale approach based on crystal plasticity is considered. The elasto-viscoplastic constitutive equations of Meric-Cailletaud are modified to take into consideration the effect of the grain size by introducing the Hall-Petch relationship at the local scale. This modified model is coupled with finite element calculations under small strain assumption to simulate the monotonic mechanical behavior of Ti-6A-4V at local and global scales. It is shown that the mechanical behavior of Ti-6Al-4V is drastically dependent upon the material features. Strong crystallographic texture can result in the formation of hardened and less hardened areas. Moreover, by increasing the grain size scattering, the heterogeneously deformed areas are multiplied. By decreasing the average grain size, the yield strength increases. It is observed that the effects of grain size, grain size scattering and crystallographic texture are coupled.

Key words: Ti-6Al-4V alloy; crystal plasticity; grain size; crystallographic texture; scattering of grain size; multi-scale modeling.

1. Introduction

Because of its high specific strength, good fatigue, and corrosion resistance Ti-6Al-4V titanium alloy is one of the most widely used materials in aeronautical and aerospace industries.

At room temperature, Ti-6Al-4V mechanical behavior is generally controlled by the behavior of α-phase (90%) since the fraction of β-phase is less than 10% [19]. The plastic strain of α-phase is accommodated by crystallographic slip mechanism because the addition of some elements such as the aluminum reduces the presence of twinning [11, 20, 21, 27, 29]. Crystallographic slip mechanism

can be hindered by various obstacles: friction of the crystalline lattice, sessile dislocations and grain boundaries.

The α- phase of Ti-6Al-4V presents a hexagonal closed packed lattice (HCP); thus, a variety of slip system families can control the plastic behavior. The grain features (size and orientation) on the one hand and the HCP lattice of the α-phase on the other hand can induce a heterogeneous and discontinuous plastic strain at the local scale which leads to an anisotropy at the global scale. Good knowledge of Ti-6Al-4V behavior is required to take into account the effects of grain dimensions as well as their scattering and their crystallographic texture on the activation of slip mechanism. In such cases, modeling based on crystal plasticity approach and scale transition rules becomes necessary.

Different phenomenological [8, 16, 17] or quasi-physical [26] models already developed can properly predict the plastic behavior of Ti-6Al-4V. Gerard *et al.* [9] have compared the reliability of the quasi-physical model of Tabourot [26] and the phenomenological model of Meric-Cailletaud [17]. They have shown that both models are able to describe the behavior of polycrystals. However, the identification of Tabourot model parameters is more difficult than that of Meric-Cailletaud model. Crystallographic texture effects have been introduced in these models through the evolution of resolved shear stress (RSS) of slip systems. Modeling of the influence of average grain size has been less reported. McDowell *et al.* [5, 16] and Fromm *et al.* [8] have introduced the role of the grain morphology on the mesoscopic behavior of Ti-6Al-4V using a local Hall-Petch relationship [13, 18] proposed by Weng [28]. Effects of scattering have been rarely investigated in Ti-6Al-4V. In most of the previous numerical contributions, the grain size distribution was considered homogeneous [8].

The aim of this work is to model the effects of the microstructural features on the monotonic tensile behavior of Ti-6Al-4V alloy. A microscopic phenomenological model in which the effect of grain size is introduced through a local Hall Petch relationship is developed. A representative elementary volume (REV) able to take into account the grain morphology and crystallographic texture is first generated, then homogenization procedure is conducted using the finite element method. The behavior is then evaluated from micro (slip system) to meso (grains size) and then at macro (REV) scales.

2. Numerical procedure

The modeling of the mechanical behavior of Ti-6Al-4V is based on a phenomenological description of crystallographic sliding in α-phase, as mentioned above. Three families of the slip system: basal $\langle a \rangle$, prismatic $\langle a \rangle$ and pyramidal $\langle c + a \rangle$ illustrated in Fig. 1 are considered. The total number of slip systems is 12 (3 basal, 3 prismatic, and 6 pyramidal).

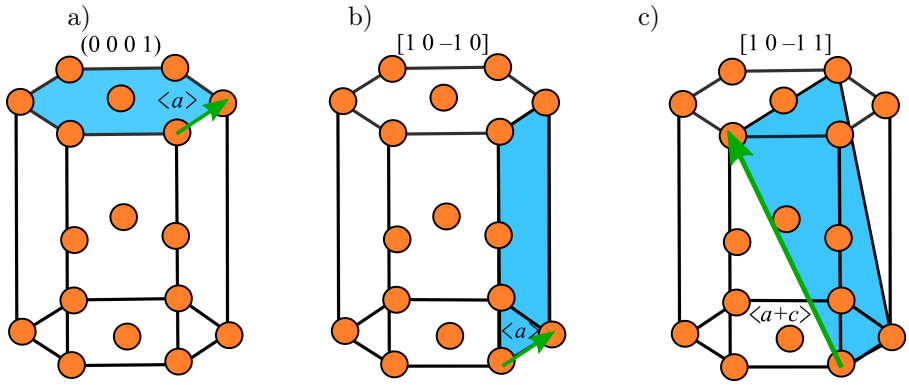

FIG. 1. Slip systems families studied in this paper: a) basal $\langle a \rangle$, b) prismatic $\langle a \rangle$, c) pyramidal $\langle c + a \rangle$.

2.1. *Constitutive law*

Modeling of crystallographic sliding activation is based on Schmid's law [25] where the resolved shear stress (RSS) of each slip system can be used as a critical variable. Thermodynamic formulation and state variables are considered to give the phenomenological description of each slip system behavior.

2.1.1. Schmid-Boas law. The RSS is given as the product of Cauchy stress tensor $\boldsymbol{\sigma}^c$ and the orientation tensor according to Schmid-Boas law [25]. For all slip strain rate in system s $|\dot{\gamma}^s| > 0$, the prescribed slip system can be activated when its resolved shear stress τ^s reaches the critical value τ_c (CRSS) as

$$\tau^s = \mathbf{n}^s \boldsymbol{\sigma}^g \mathbf{m}^s \geq \tau_c^s, \tag{2.1}$$

where $\boldsymbol{\sigma}^g$ is the stress tensor applied on grain g, $\mathbf{n}^s$, and $\mathbf{m}^s$ are the normal and the direction of slip plane s respectively.

2.1.2. Formulation of local behavior model. In the Meric-Cailletaud model [17], the slip strain rate $\dot{\gamma}^s$ of a given system s is described by a power function of the resolved shear stress τ^s as

$$\dot{\gamma}^s = \dot{v}^s \operatorname{sign}(\tau^s - \chi^s), \tag{2.2}$$

with

$$\dot{v}^s = \left\langle \frac{|\tau^s - \chi^s| - r^s}{K} \right\rangle^n. \tag{2.3}$$

The $\langle . \rangle$ is Macaulay brackets defined as

$$\langle x \rangle = \left\{ \begin{array}{ll} 0, & x < 0 \\ x, & x \geq 0 \end{array} \right\}.$$

χ^s and r^s are the kinematic and the isotropic hardening variables of slip system s, respectively, τ^s is the resolved shear stress of system s, K, and n characterize the material viscosity. The isotropic hardening variable r^s describes the expansion of the elastic behavior domain, and its initial value gives the critical resolved shear stress τ_c^s. This variable introduces the interaction between slip systems via a hardening matrix. Its exponential form allows a nonlinear saturation of critical resolved shear stress (CRSS):

$$r^s = \tau_c^s + Q \sum_r h^{rs}(1 - e^{-b\rho}), \tag{2.4}$$

with

$$\dot{\rho}^s = (1 - b\rho^s)\dot{v}^s, \tag{2.5}$$

where b and Q represent the material sensibility to the saturation and the isotropic hardening rate respectively, h^{rs} is a hardening matrix and ρ is an internal state variable describing the evolution of isotropic hardening in system s.

Moreover, the nonlinear kinematic hardening of slip systems describes the Bauschinger effect observed in macroscopic hysteresis loops resulted from the internal stresses at the mesoscopic scale. It is given according to the Armstrong-Frederick form [7]:

$$\chi^s = C\alpha^s, \tag{2.6}$$

with

$$\dot{\alpha}^s = \dot{\gamma}^s - d\alpha^s\dot{\chi}^s, \tag{2.7}$$

where α^s is an internal state variable describing the evolution of kinematic hardening in slip system s, C and d are material parameters.

2.1.3. Hall-Petch relationship. In order to take into account the effect of grain size of the α phase, the Hall-Petch relationship [13, 18] is introduced in the local model when calculating the critical resolved shear stress τ_c^s of each slip systems as

$$\tau_c^s = \tau_0^s + K_{hp}\frac{1}{\sqrt{D}}, \tag{2.8}$$

where D is the average diameter of grain g, K_{hp} is the Hall-Petch slope, and τ_0 is a constant of lattice friction depending on c/a ratio in HCP materials.

2.2. Ti-6Al-4V microstructure

Generation of Ti-6Al-4V microstructure is performed using an open source software Neper [22]. It consists in generating a REV able to represent the microstructural features of the equiaxed α grains.

2.2.1. Generation of the morphology. Four REVs with the size of $(120 \times 120 \times 120)$ μm^3 are generated (see Table 1). Equiaxed grains are considered using Voronoi tessellations approach.

Table 1. Different cases of generated REV morphology.

REV	Grain number	Grain size [μm]	Scattering
1	1900	3	$\Delta D/D = 0$
2	300	14	$\Delta D/D = 0$
3	1900	3	$\Delta D/D = 2.5$
4	300	14	$\Delta D/D = 2.5$

The generated REVs allow to study two average grain sizes: 3 μm and 14 μm with two scatterings: $\Delta D/D = 0$ (Dirac distribution) and $\Delta D/D = 2.5$ (log-normal distribution), where ΔD defines the difference between the size of the largest ($D_{\max}$) and the smallest grains ($D_{\min}$) as $\Delta D = D_{\max} - D_{\min}$. The generated REVs as well as the proposed scattering functions are illustrated in Figs 2 and 3 respectively.

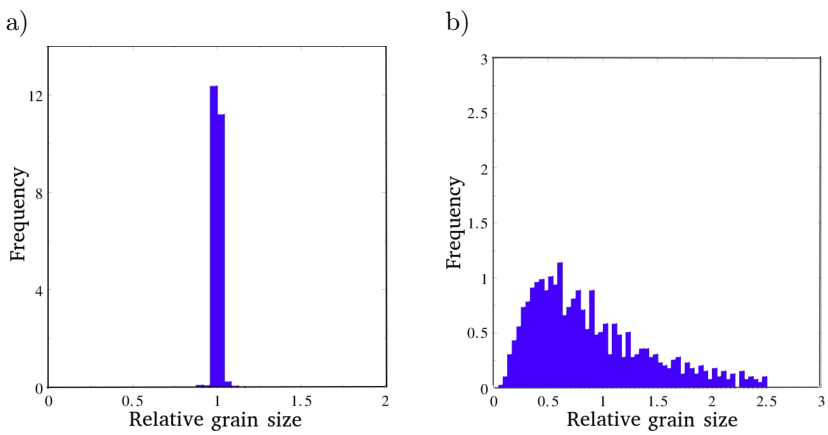

FIG. 2. Grain size distribution: a) Dirac $\Delta D/D = 0$, b) log-normal $\Delta D/D = 2.5$.

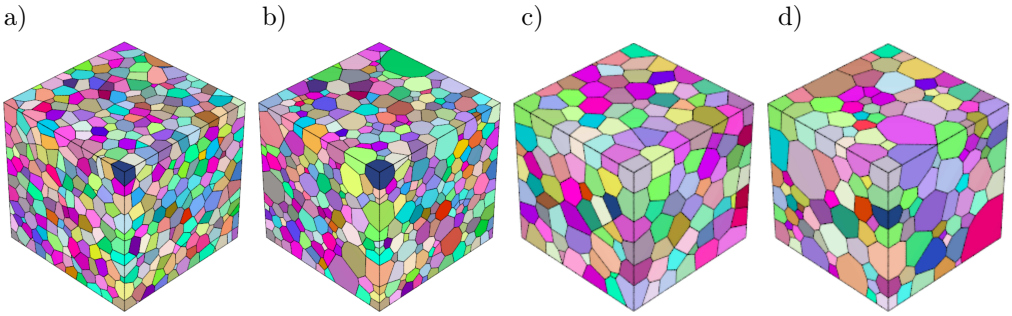

FIG. 3. Generated REVs: a) 1900 grains with Dirac scattering $\Delta D/D = 0$, b) 1900 grains with log-normal scattering $\Delta D/D = 2.5$, c) 300 grains with Dirac scattering $\Delta D/D = 0$, and d) 300 grains with log-normal scattering $\Delta D/D = 2.5$.

It should be noted that the minimal number of grains (300) is optimized to be representative in order to avoid any effect of grains number. Moreover, the time needed to generate the REVs strongly depends on the number of grains, it is about 2 hours in the case of 1900 grains and 20 min in the case of 300 grains. Sphericity distribution of equiaxed grain shape is also considered (see Fig. 4).

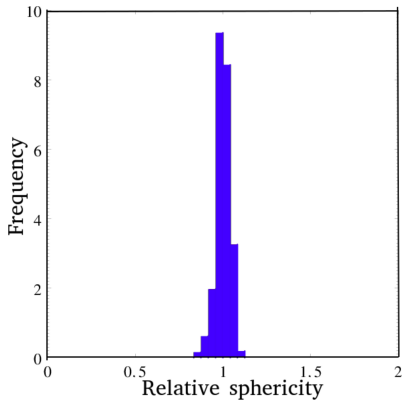

FIG. 4. Statistical analysis of the grains sphericity distribution.

2.2.2. Generation of crystallographic texture. Figure 5 shows three crystallographic textures that are generated and illustrated as pole figures using Mtex-Matlab toolbox. Tx1 displays a relatively weak texture where the grains are randomly oriented, this allows to consider Ti-6Al-4V as an isotropic material. Tx2 reflects an intermediate textured material. Tx3 considers a strong textured material where all grains have the same crystallographic orientation, and the material is thus strongly anisotropic.

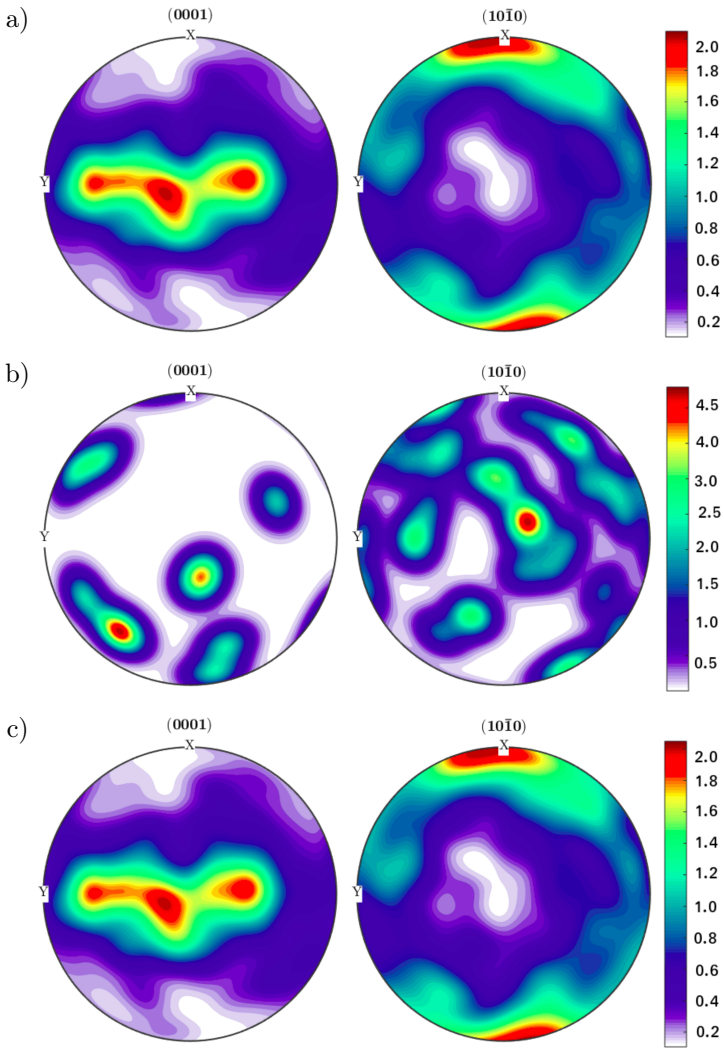

FIG. 5. Pole figures of modeled Ti-6Al-4V alloy in different product forms: a) Tx1, b) Tx2, and c) Tx3.

2.3. Meshing and boundary conditions

Meshing techniques proposed by QUEY *et al.* [22] and available in Neper are adopted. Quadratic tetrahedral meshing elements (C3D10) are used with a mean size of 1.25 μm (about 115 960 elements per REV). The number of elements per grain depends on the given average grain size of each generated RVE as well as their scattering (Table 1). It is approximately the same in the case of Ti-6Al-4V with Dirac distribution ($\Delta D/D = 0$). However, in the case of log-normal distribution ($\Delta D/D = 2.5$), the number of mesh elements strongly varies from

a Voronoi cell to another in the same RVE. The mean number N_e^m, the maximum number $N_e^{\max}$ and the minimum number $N_e^{\min}$ of mesh elements per grain are presented in Table 2. The mesh elements of a given REV are shown in Fig. 6a.

Table 2. Grains meshing details.

Conditions	N_e^m/grain	$N_e^{\min}$/grain	$N_e^{\max}$/grain
3 µm; Dirac distribution	61	52	73
3 µm; Log-N distribution	61	16	108
14 µm; Dirac distribution	382	343	402
14 µm; Log-N distribution	370	204	534

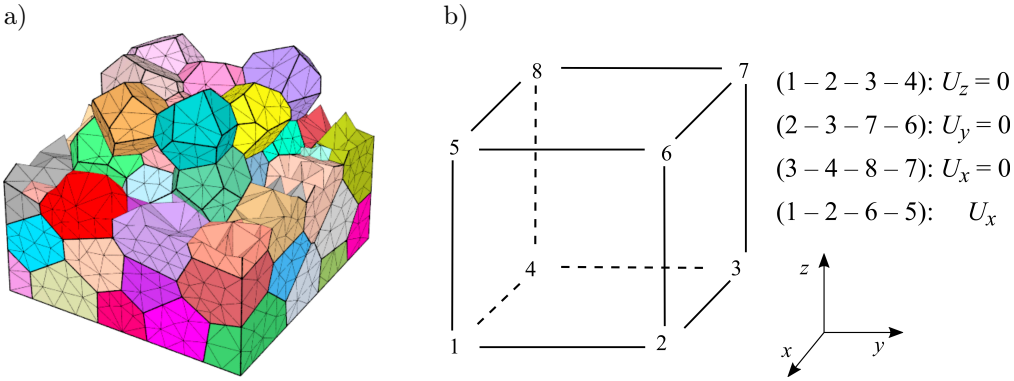

Fig. 6. Meshing (a) and applied boundary conditions (b).

The boundary conditions consider retained displacements on three faces with symmetrical conditions, and a displacement loading is applied to one of the free faces according to the x-axis to obtain 2% of strain as illustrated in Fig. 6b.

3. Results and discussion

For each condition illustrated in Table 1, three initial textures are considered, which leads to 12 finite element numerical simulations performed using Zmat library [3, 4]. The model behavior parameters have been proposed by Dick *et al.* [6] for equiaxed Ti-6Al-4V alloy (Table 3) where B, P, and π denote respectively basal $\langle a \rangle$, prismatic $\langle a \rangle$, and pyramidal $\langle c + a \rangle$ slip systems. The Hall-Petch slopes are considered to be the same for all slip systems [16]. In the present study, 2 processors with a clock rate of 2.8 GHz and a random access memory (RAM) of 30 GB per node are considered for each calculation.

Table 3. Material parameters of Ti-6Al-4V [6], Hall-Petch constants [16].

E [MPa]	v	b	C [MPa]	d	n	K [MPa·s$^{1/n}$]	Q [MPa]			τ_0 [MPa]			K_{hp} [MPa·µm$^{-1/2}$]
							B	P	π	B	P	π	
119000	0.29	2	30.000	300	7.41	20	−49	−52	−83	394	380	630	17

3.1. Analysis of mechanical behavior at macroscopic scale

3.1.1. Grain size effects. Figure 7a shows that the grain size influences the yield strength of the isotropic Ti-6Al-4V alloy (Tx1), by increasing the average grain size, the yield strength decreases. However, when the Ti-6Al-4V becomes more textured (Tx2), the grain size effects decrease (Fig. 7b). Here, the yield strength seems to be dependent on the grain size, but the hardening has a tendency to reduce this effect. For Ti-6Al-4V strongly textured (Tx3), it is observed that there is no effect of grain size on Ti-6Al-4V

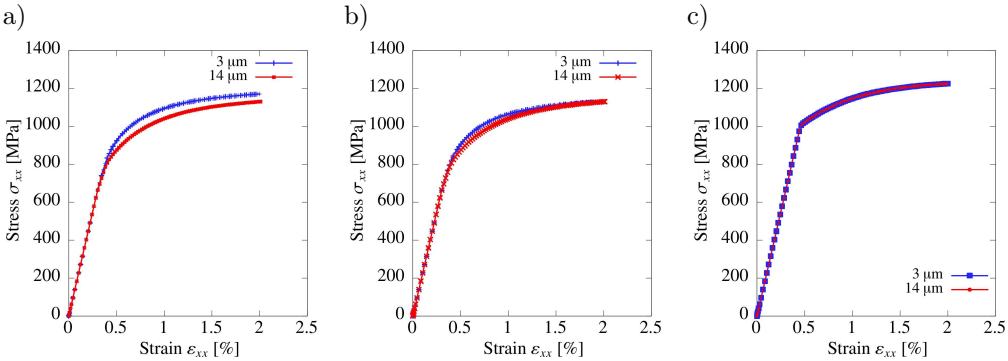

FIG. 7. Influence of grain size on Ti-6Al-4V mechanical behavior when $\Delta D/D = 0$ and the crystallographic texture is: a) Tx1, b) Tx2, c) Tx3.

3.1.2. Influence of grain size scattering. A considerable influence of grain size scattering is seen for an average grain size about of 3 µm (Fig. 8a). However, by increasing the grain size, the effect of scattering decreases (Fig. 8b). This can be confirmed by analyzing the Hall-Petch law at the macroscopic scale that gives the relationship between the macroscopic yield strength σ_y and the average grain size D. By increasing the average grain size, the ratio $(K_{hp}/\sqrt{D})$ is getting closer to 0 regardless of the scattering. Therefore, the yield strength tends towards the same value (Fig. 8b). Similar results have been shown in other investigation for polycrystal materials [1, 2, 23].

3.1.3. Crystallographic texture effects. Figure 9 shows that the yield strength and the hardening are strongly influenced by the crystallographic texture. For

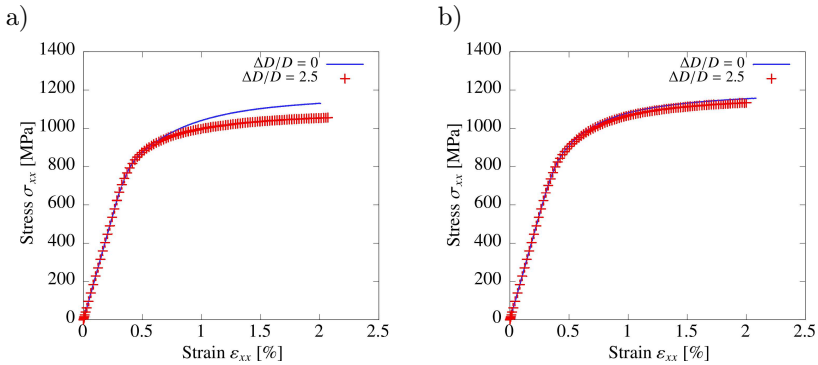

FIG. 8. Effect of grain size scattering on isotropic Ti-6Al-4V mechanical behavior when the average grain size is (a) 3 µm and (b) 14 µm.

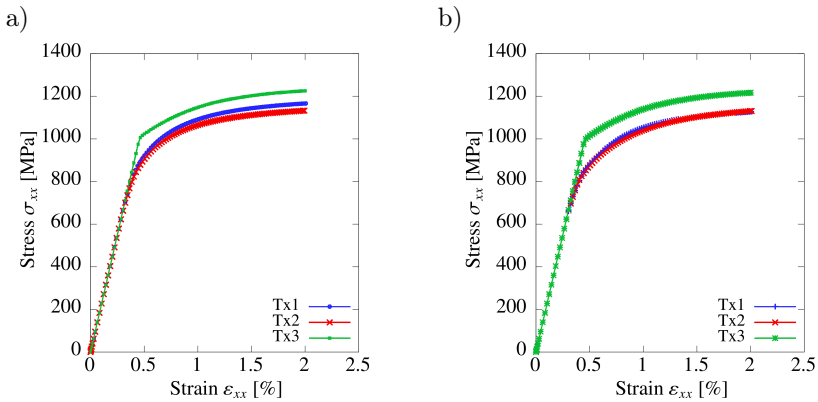

FIG. 9. Influence of crystallographic texture on Ti-6Al-4V behavior when $\Delta D/D = 0$ and grain size is (a) 3 µm, (b) 14 µm.

weakly (Tx1) and intermediate (Tx2) textured materials, the effects of crystallographic texture appear when the average grain size decreases.

3.1.4. Role of the crystallographic slip mechanism. For each texture, a Schmid factor is calculated for basal $\langle a \rangle$, prismatic $\langle a \rangle$, and pyramidal $\langle c{+}a \rangle$ slip systems and presented in Fig. 10. This figure gives an idea of the percentage of grains favorably oriented for a given sliding family (their Schmid factor $SF_0 \geq 0.4$). The ability to activate a slip system increases when its Schmid factor increases. However, the CRSS is different from one family to another with ratios of $\frac{\tau_c^P}{\tau_c^P}$: $\frac{\tau_c^B}{\tau_c^P}$: $\frac{\tau_c^{Py}}{\tau_c^P} = 1 : 1.05 : 1.68$ for prismatic $\langle a \rangle$, basal $\langle a \rangle$, and pyramidal $\langle c + a \rangle$ systems respectively [6]. The pyramidal family $\langle c + a \rangle$ may be activated only when grains are favorably oriented; thus, the plastic strain is mainly controlled by prismatic $\langle a \rangle$ and basal $\langle a \rangle$ systems.

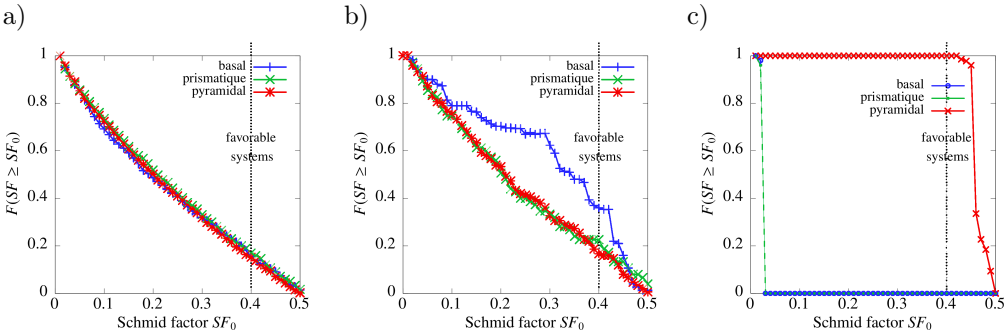

FIG. 10. Cumulative distribution $F(SF \geq SF_0)$ of Schmid factors of basal $\langle a \rangle$ prismatic $\langle a \rangle$ and pyramidal $\langle c+a \rangle$: a) Tx1, b) Tx2, c) Tx3. The representation of the distribution is chosen so that the ordinate of a point SF_0 gives the frequency F of grains having a Schmid factor greater or equal to SF_0.

The relative amount of the activated slip systems during tensile loading is shown in Fig. 11. When Ti-6Al-4V is textured with Tx1 and Tx2, prismatic and basal systems start to be activated locally after 0.2% of total strain while the material always exhibits a macroscopic elastic behavior. Dislocations movement in pyramidal systems is activated after 0.5% of strain. When the total deformation reaches 2%, about 40.34% of prismatic, 28.33% of basal and 10% of pyramidal systems are activated. Only 20% of prismatic systems have a Schmid factor larger than 0.4 (Fig. 10), which indicates that these systems can be activated with small Schmid factors. The plastic strain is accommodated by pyramidal $\langle c+a \rangle$ systems only when Tx3 is considered. Here, the loading axis is perpendicular to the slip direction $\langle a \rangle$ (see Fig. 1).

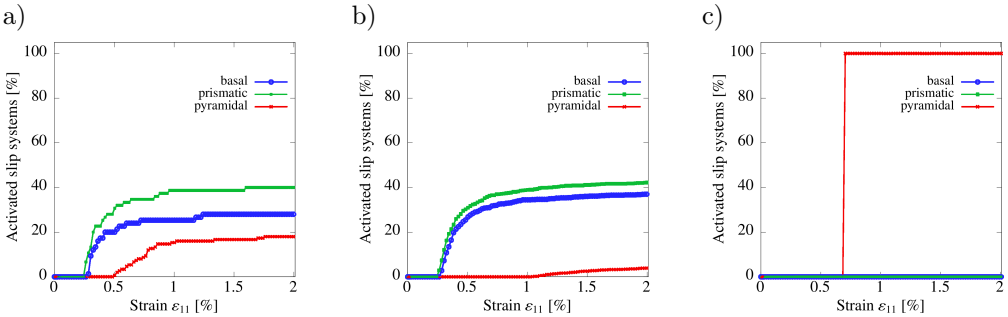

FIG. 11. Variation of activated slip systems of basal $\langle a \rangle$, prismatic $\langle a \rangle$ and pyramidal $\langle c+a \rangle$ families during tensile loading: a) Tx1, b) Tx2, c) Tx3.

It should be noted that Schmid factors only depend on the initial crystallographic texture. The small strain assumption considered in this paper allows to suppose that there is no evolution of crystallographic texture during tensile tests. Moreover, the CRSS depends on the size of each individual grain which means

that the activation of slip systems of the same family can change according to both crystallographic texture and individual grain size.

3.2. Analysis of mechanical behavior at mesoscopic scale

For the two scatterings of grain size: $\Delta D/D = 0$ and $\Delta D/D = 2.5$, the local tensile stress $\sigma_{xx} - \varepsilon_{xx}$ curves of 8 randomly selected grains are presented in Figs 12 and 13. When Ti-6Al-4V is textured with Tx1 and Tx2, an important heterogeneity of local behavior is shown in both $\Delta D/D = 0$ and $\Delta D/D = 2.5$. Coarse grains can easily deform compared to small grains. The fast interaction between mobile dislocations and grain boundaries in small grains leads to a stress concentration, which induces a significant hardening. However, the local behavior becomes more homogeneous when the material is textured with Tx3 (see Figs 12c and 13c). Similar results have also been reported in previous studies [10, 12, 15, 24]. Figures 14 and 15 illustrate the maps of Huber-Mises stress [14] when the average grain size of Ti-6Al-4V is 3 µm and 14 µm, respectively. When the material is textured with Tx1, a significant stress heterogeneity is shown

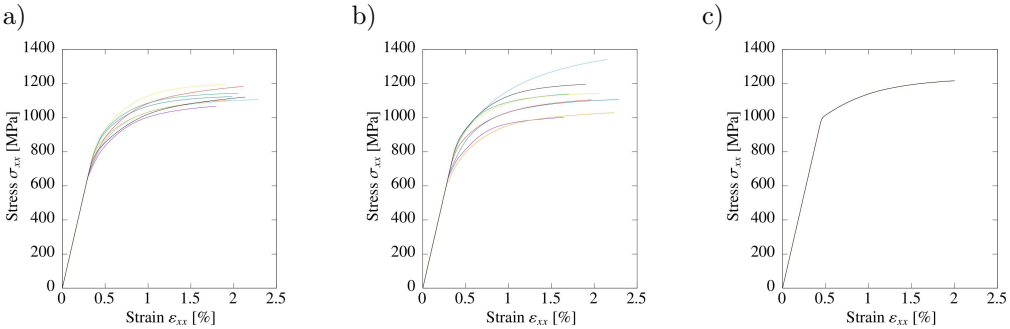

FIG. 12. Local stress-strain curves of REV grains generated with scattering $\Delta D/D = 0$, the average grain size of 14 µm and: a) Tx1, b) Tx2, c) Tx3.

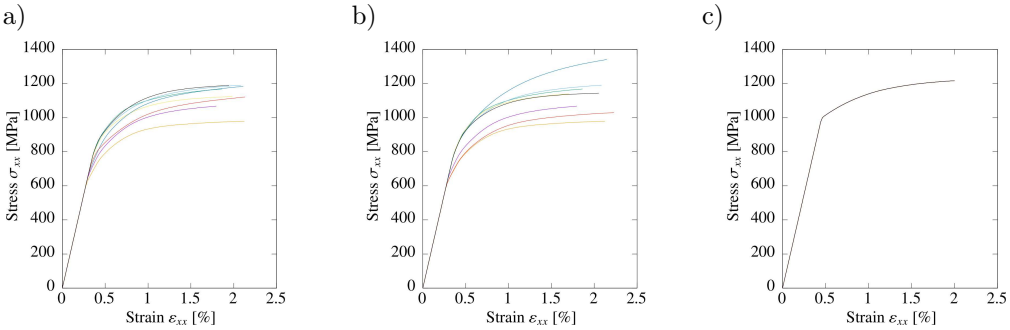

FIG. 13. Local stress-strain curves of REV grains generated with scattering $\Delta D/D = 2.5$, the average grain size of 14 µm and: a) Tx1, b) Tx2, c) Tx3.

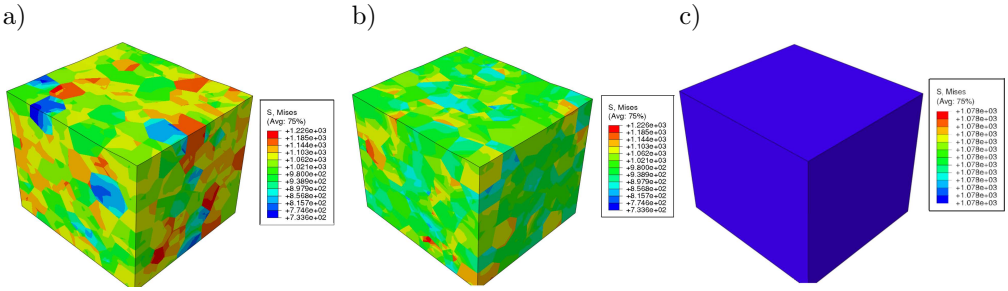

FIG. 14. Equivalent Huber-Mises stress map of Ti-6Al-4V REV generated with scattering $\Delta D/D = 2.5$, the grain size of 3 μm and: a) Tx1, b) Tx2, c) Tx3.

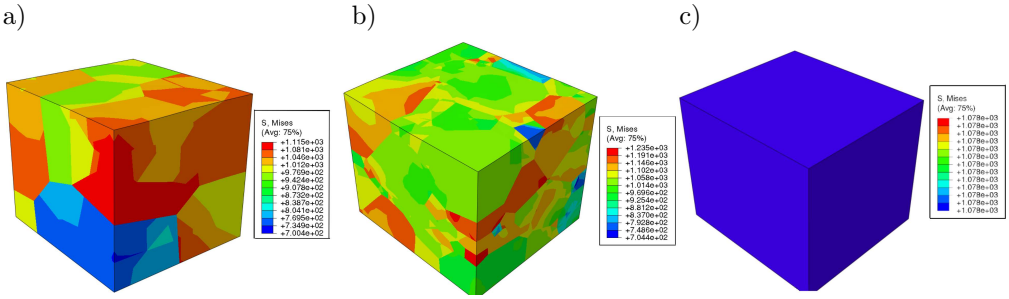

FIG. 15. Equivalent Huber-Mises stress map of Ti-6Al-4V REV generated with scattering $\Delta D/D = 2.5$, the grain size of 14 μm and: a) Tx1, b) Tx2, c) Tx3.

(Figs 14a and 15a) mainly resulting from the random crystallographic orientations. The distribution of stresses becomes more homogeneous when the material is textured with Tx2 and especially when grain size decreases (Figs 14b and 15b). When Ti-6Al-4V is strongly textured (Tx3), a homogeneous distribution of stress is observed in both average grain sizes (Figs 14c and 15c).

4. Summary and conclusions

A phenomenological crystal plasticity model has been developed to investigate the role of Ti-6Al-4V microstructural features on the accommodation of plastic behavior at macroscopic (REV) and mesoscopic (grains) scales during tensile loading. The main conclusions of this research are summarized as follows:

- The grain orientation is shown to have a significant effect on the local and global mechanical behavior of Ti-6Al-4V.
- Coupling between the effects of average grain size, scattering and crystallographic texture is observed. The crystallographic texture effects are

influenced by the average grain size. Moreover, the role of scattering is shown when the average grain size decreases.

- The effects of grain size can be influenced by the initial crystallographic texture. When the material is strongly textured (all grains have the same crystallographic orientation), the material can be considered as a monocrystal with no effects of the morphology.

Acknowledgments

The authors would like to thank the French Occitanie region and IMT-Mines Albi for their financial supports.

References

1. Berbenni S., Favier V., Berveiller M., *Impact of the grain size distribution on the yield stress of heterogeneous materials*, International Journal of Plasticity, **23**(1): 114–142, 2007.

2. Berbenni S., Favier V., Berveiller M., *Micro-macro modelling of the effects of the grain size distribution on the plastic flow stress of heterogeneous materials*, Computational Materials Science, **39**(1): 96–105, 2007.

3. Besson J., Foerch R., *Large scale object-oriented finite element code design*, Computer Methods in Applied Mechanics and Engineering, **142**(1–2): 165–187, 1997.

4. Besson J., Leriche R., Foerch R., Cailletaud G., *Object-oriented programming applied to the finite element method. Part II. Application to material behaviors*, Revue Européenne des Éléments Finis, **7**(5): 567–588, 1998, https://doi.org/10.1080/12506559.1998.10511322.

5. Bridier F., McDowell D., Villechaise P., Mendez J., *Crystal plasticity modeling of slip activity in Ti-6Al-4V under high cycle fatigue loading*, International Journal of Plasticity, **25**(6): 1066–1082, 2009.

6. Dick T., Cailletaud G., *Fretting modelling with a crystal plasticity model of Ti6Al4V*, Computational Materials Science, **38**(1): 113–125, 2006.

7. Frederick C.O., Armstrong P.J., *A mathematical representation of the multiaxial Bauschinger effect*, Materials at High Temperature, **24**(1): 1–26, 2007.

8. Fromm B.S, Adams B.L., Ahmadi S., Knezevic M., *Grain size and orientation distributions: Application to yielding of α-titanium*, Acta Materialia, **57**(8): 2339–2348, 2009.

9. Gerard C., *Field measurements and evaluation of crystal plasticity models* [in French: *Mesures de champs et identiffication de modéles de plasticité cristalline*], PhD thesis, École Polytechnique, 91128 Palaiseau Cedex, France, 2008.

10. Germain L., Gey N., Humbert M., Bocher P., Jahazi M., *Analysis of sharp microtexture heterogeneities in a bimodal IMI 834 billet*, Acta Materialia, **53**(13): 3535–3543, 2005.

11. Gilles G., Hammami W., Libertiaux V., Cazacu O., Yoon J.H., Kuwabara T., Habraken A.M., Duchêne L., *Experimental characterization and elasto-plastic modeling of the quasi-static mechanical response of TA-6 V at room temperature*, International Journal of Solids and Structures, **48**(9): 1277–1289, 2011.

12. Glavicic M.G., Bartha B.B., Jha S.K., Szczepanski C.J., *The origins of microtexture in duplex Ti alloys*, Materials Science and Engineering: A, **513–514**: 325–328, 2009.

13. Hall E.O., *The deformation and ageing of mild steel: III Discussion of results*, Proceedings of the Physical Society, Section B, **64**(9): 747–753, 1951.

14. Huber M.T., *Speciffic work of strain as a measure of material effort*, Archive of Mechanics, **56**(3): 173–190, 2004 (originally Czasopismo Techniczne, XXII, 1904, Lwów, Proceedings of Lwów Polytechnic Society; translated into English in 2004 by A. Stręk under scientific supervision of R.B. Pęcherski).

15. Lunt D., da Fonseca Q.D., Rugg D., Preuss M., *Microscopic strain localisation in Ti-6Al-4V during uniaxial tensile loading*, Materials Science and Engineering: A, **680**: 444–453, 2017.

16. Mayeur J.R., McDowell D.L., *A three-dimensional crystal plasticity model for duplex Ti-6Al-4V*, International Journal of Plasticity, **23**(9): 1457–1485, 2007.

17. Méric L., Poubanne P., Cailletaud G., *Single crystal modeling for structural calculations: Part 1 – Model presentation*, Engineering Materials and Technology, **113**(1): 162–170, 1991.

18. Petch N.J., *The cleavage strength of polycrystals*, Journal of the Iron and Steel Institute, **174**: 25–28, 1953.

19. Philippe M.J., Bouzy E., Fundenberger J.-J., *Textures and anisotropy of titanium alloys*, Materials Science Forum, **273–275**: 511–522, 1998.

20. Philippe M.J., Esling C., Hocheid B., *Role of twinning in texture development and in plastic deformation of hexagonal materials*, Textures, Stress, and Microstructures, **7**(4): 265–301, 1988.

21. Philippe M.J., Serghat M., Van Houtte P., Esling C., *Modelling of texture evolution for materials of hexagonal symmetry. II. Application to zirconium and titanium αor near α-alloys*, Acta Metallurgica et Materialia, **43**(4): 1619–1630, 1995.

22. Quey R., Dawson P.R., Barbe F., *Large-scale 3D random polycrystals for the finite element method: Generation, meshing and remeshing*, Computer Methods in Applied Mechanics and Engineering, **200**(17–20): 1729–1745, 2011.

23. Ramtani S., Bui H.Q., Dirras G., *A revisited generalized self-consistent polycrystal model following an incremental small strain formulation and including grain-size distribution effect*, International Journal of Engineering Science, **47**(4): 537–553, 2009.

24. Rugg D., Dixon M., Dunne F.P.E., *Effective structural unit size in titanium alloys*, The Journal of Strain Analysis for Engineering Design, **42**(4): 269–279, 2007.

25. Schmid E., Boas W., *Crystal plasticity* [in German: *Kristallplastizität*], Verlag Julius Springer, Berlin, 1935.

26. Tabourot L., Fivel M., Rauch E., *Generalised constitutive laws for f.c.c. single crystals*, Materials Science and Engineering: A, **234–236**: 639–642, 1997.

27. Tirry W., Coghe F., Bouvier S., Gasperini M., Rabet L., Schryvers D., *A multi-scale characterization of deformation twins in Ti6Al4V sheet material deformed by simple shear*, Materials Science and Engineering: A, **527**(16–17): 4136–4145, 2010.

28. Weng G.J., *A micromechanical theory of grain-size dependance in metal plasticity*, Journal of the Mechanics and Physics of Solids, **31**(3): 193–203, 1983, https://doi.org/10.1016/0022-5096(83)90021-2.

29. Williams J.C., Baggerly R.G., Paton N.E., *Deformation behavior of HCP Ti-Al alloy single crystals*, Metallurgical and Materials Transactions A, **33**(3): 837–850, 2002.

Received December 31, 2018; accepted version April 8, 2018.

Published on Creative Common licence CC BY-SA 4.0